Applied Physics Letters ARTICLE scitation.org/journal/apl

Reverse leakage and breakdown mechanisms of vertical GaN-on-Si Schottky barrier diodes with and without implanted termination

Cite as: Appl. Phys. Lett. **118**, 243501 (2021); doi: 10.1063/5.0049706
Submitted: 8 March 2021 · Accepted: 30 May 2021 ·
Published Online: 14 June 2021

Xiaolu Guo,[1,2] Yaozong Zhong,[2,3] Xin Chen,[2] Yu Zhou,[1,2,3,a)] Shuai Su,[1,2] Shumeng Yan,[1,2] Jianxun Liu,[2,3] Xiujian Sun,[2] Qian Sun,[1,2,3,a)] and Hui Yang[1,2,3]

AFFILIATIONS

[1]School of Nano Technology and Nano Bionics, University of Science and Technology of China, Hefei 230026, People's Republic of China
[2]Key Laboratory of Nano-Devices and Applications, Suzhou Institute of Nano-Tech and Nano-Bionics, Chinese Academy of Sciences (CAS), Suzhou 215123, People's Republic of China
[3]Suzhou Institute of Nano-Tech and Nano-Bionics, CAS, Foshan 528000, People's Republic of China

[a)]**Authors to whom correspondence should be addressed:** yzhou2008@sinano.ac.cn and qsun2011@sinano.ac.cn

ABSTRACT

This Letter studies the reverse leakage and breakdown mechanisms of vertical GaN-on-Si Schottky barrier diodes (SBDs) with and without argon-implanted termination (ArIT). The electrical leakage characteristics in the vertical GaN-on-Si SBD without edge termination sequentially go through the thermionic field emission, variable range hopping (VRH), and trap-assisted tunneling conduction mechanisms as the reverse bias increases gradually. Its leakage and breakdown mechanisms are limited by the edge electric field crowding effect. While for the vertical GaN-on-Si SBD with ArIT (ArIT-SBD), the electrons conduction at a low reverse bias, following the space-charge-limited conduction (SCLC) model, is limited by the damage-induced traps in the implanted GaN. As the reverse bias increases up to the occurrence of breakdown, the VRH and SCLC dominate the leakage mechanism of the ArIT-SBD, which stem from intrinsic traps in GaN grown on Si. A rapidly growing leakage under a low reverse bias and enhanced breakdown voltage performance in the ArIT-SBD is attributed to the charging of the damage-induced traps in implanted GaN. This Letter not only gives in-depth insights of vertical GaN-on-Si SBDs but also provides a useful design guidance of implanted termination for high-voltage power devices.

GaN-based vertical power devices,[1] with the capability of high output power, excellent thermal management, and superior dynamic performance, have become desirable for the next-generation power applications. Due to the huge development of the epitaxy material technology, vertical GaN power devices on freestanding substrates have had an impressive record of achievements, such as current-collapse-free 800-V Schottky barrier diodes (SBDs),[2] 1200-V PIN diodes, and junction FEs (JFETs) with avalanche ruggedness.[3,4] Recently, GaN (quasi-) vertical power devices grown on low-cost and large-size Si substrates hold the huge potential for various applications.[5] An impressive record has been made for vertical GaN-on-Si power devices, such as 820-V PIN diodes with a high Baliga's figure of merit of 2 GW/cm^2,[6] 520-V power MOSFETs.[7] Thanks to its high switching frequency and low energy loss,[8–10] vertical GaN-on-Si SBDs have attracted much attention, and a high breakdown voltage (BV) of ~400 V has been realized with a 3-μm-thick drift layer.[11] Compared with vertical GaN-on-GaN SBDs, the high off-state leakage current and moderate BV limit the application of vertical GaN-on-Si SBDs. However, few works have studied the reverse leakage of GaN-on-Si vertical SBDs in detail; the reverse leakage and breakdown mechanisms of vertical GaN-on-Si SBDs are not clear to date.

Given the capability to alleviate the crowding electric field effect and avoid the premature breakdown of power devices,[8] edge termination (ET) technology is a key topic for high-voltage SBDs. With high throughput and easy implementation,[10] ion-implanted termination has become one of the most promising ET technologies for realizing the high-voltage power devices and has been applied widely in GaN or Ga_2O_3 power devices.[10–16] Implanted termination could greatly promote the breakdown voltage of power devices, but meanwhile, it may result in a growing on-resistance,[10–14] or a rapidly growing current at

a low reverse bias (V_R).[10,11,14–16] These phenomena indicate that the implanted termination may have dramatically affected leakage and breakdown mechanisms of vertical power devices. In fact, the impact of implanted terminations on forward electrical characteristics of vertical SBDs has been reported,[12] but not on the reverse electrical behavior.

In this work, the leakage and breakdown mechanisms of vertical GaN-on-Si SBDs with and without argon-implanted termination are demonstrated clearly. By directly comparing the leakage mechanisms of SBDs with and without implanted termination, the impact of the implanted termination on the reverse electrical characteristics of vertical SBDs has been unveiled.

As shown in Fig. 1(a), the GaN SBD structure was grown on a Si(111) substrate with AlN/AlGaN stress engineering buffer layers by metal-organic chemical deposition (MOCVD).[17,18] It consisted of a 3-μm-thick high-quality n^--GaN drift layer (N_D–$N_A \approx 2.1 \times 10^{16}\,cm^{-3}$) and a 1-$\mu$m-thick n^+-GaN current spreading layer ($N_D \approx 5 \times 10^{18}\,cm^{-3}$). The argon ion implantation with an energy of 50 keV at a dose of $1 \times 10^{16}\,cm^{-2}$ was performed using the anode metal directly as a mask. As shown in Fig. 1(b), the argon ion profile by the SIMS measurement shows a full width at half maximum (FWHM) of ~40 nm. The detailed fabrication process of the GaN SBD with an ArIT could be referred to our previous report.[11] The reference SBD (Ref-SBD) was fabricated by the same process except for the absence of the ArIT.

Figure 1(c) shows the forward I–V characteristics and differential specific on-resistance (R_{on}) of the Ref-SBD and ArIT-SBD. The optimized forward I–V curves could be expressed by the thermionic emission model

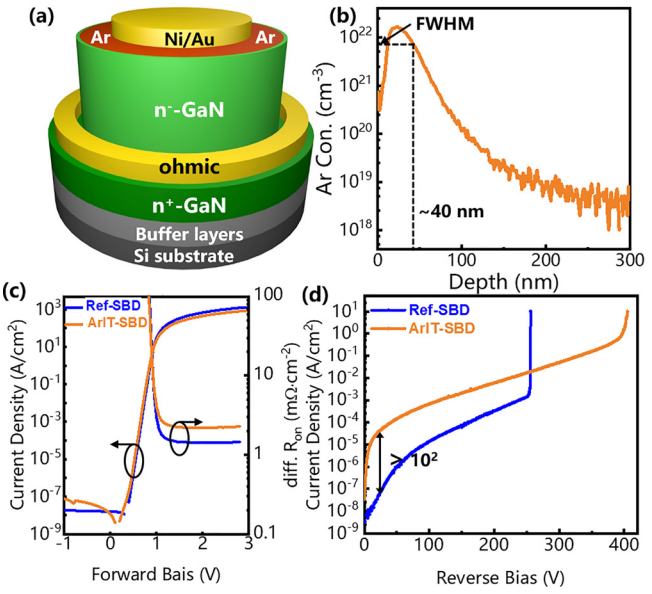

FIG. 1. (a) 3D schematic of the as-fabricated quasi-vertical GaN-on-Si ArIT-SBD. (b) SIMS ions profile along the vertical direction in the argon-implanted GaN. (c) Forward I–V characteristics and differential R_{on} and of the Ref-SBD and ArIT-SBD. (d) Reverse I–V characteristics of the Ref-SBD and ArIT-SBD.

$$J_{TE} = A^* T^2 \exp\left(-\frac{\phi_B}{kT}\right)\left(\frac{q(V - JR_s)}{\eta kT}\right),$$

where A^* is the effective Richardson constant (theoretically 26.4 A/cm^2·K^2 for GaN),[19] ϕ_B is the Schottky barrier height, R_s is the series resistance, and η is the ideality factor. Both the Ref-SBD and ArIT-SBD achieve an output current density of ~kA/cm^2 at +3 V and a low leakage current up to 1×10^7 A/cm^2 at a V_R of −1 V, giving a high current on/off ratio of ~10^{10}. The extracted ideality factors of the Ref-SBD and ArIT-SBD are 1.03 and 1.04, respectively. The high current on/off ratio and the near-unity ideality factor reflect the high-quality Ni/n^--GaN interface and n^--GaN drift layer with a low density of threading dislocations.[8,11] Compared with the Ref-SBD with a R_{on} of 1.41 mΩ cm^2, the ArIT-SBD has a slightly larger R_{on} of 2.22 mΩ·cm^2 [Fig. 1(c)]. The increased R_{on} should be ascribed to the suppressed current spreading laterally,[20] related to the compensation effect of the damage-related traps induced by the argon ion implantation.[11,21]

As shown in Fig. 1(d), the ArIT boosts the BV of the GaN-on-Si vertical SBD from ~250 to 405 V, yielding a high critical electric field of ~2 MV/cm. However, the introduction of the ArIT leads to a rapidly growing reverse leakage current at V_R of 10 V by more than two orders of magnitude. The temperature-dependent (T-dependent) I–V measurements for both the ArIT-SBD and Ref-SBD were performed to study its leakage and breakdown mechanisms.

As shown in Fig. 2(a), according to dependence of the distinct leakage behaviors on both the temperature and reverse bias,[19] the reverse I–V curves of the Ref-SBD could be divided into three zones. Under a low V_R of ~10 V (zone I), the electrode-limited conduction often dominates the carrier transport in the vertical SBD under a low electric field,[22] such as thermionic emission (TE) or thermionic field emission (TFE),[23] as depicted in Fig. 2(e). For the Ref-SBD, the I–V curves measured at various low temperatures (≤125 °C) present an excellent agreement with the theoretical fitting results [Fig. 2(b)] based on the TFE model, as described by the equation

$$J_{TFE} = \frac{A^* The E}{2\pi k}\sqrt{\frac{\pi}{2m_n^* kT}} \times \exp\left[-\frac{1}{kT}\left(\varnothing_b - \frac{(ehE)^2}{24m_n^*(2\pi kT)^2}\right)\right],$$

where E is the critical electric field at the Schottky junction interface and is given by

$$E = \sqrt{\frac{2e(N_D - N_A)(V_R + V_{bi})}{\varepsilon_s}},$$

where $\varnothing_b$ is the Schottky barrier height, m_n^* is the effective electron mass for GaN, and ε_s is the dielectric constant of GaN. The well-fitted results verify that the TFE conduction is the dominant leakage mechanism.

When a V_R increases up to 80 V for the Ref-SBD (zone II, the corresponding calculated E is up to 0.8 MV/cm), the linear relationship between ln$J$ and E [Fig. 2(c)] indicates that the reverse leakage is mainly dominated by the variable range hopping (VRH) process,[24] as shown in Fig. 2(f). The electrons injected from the Schottky contact hop from one trap to another successively through the defects mini-band of the bulk GaN.[25] The VRH model expression could be shown by

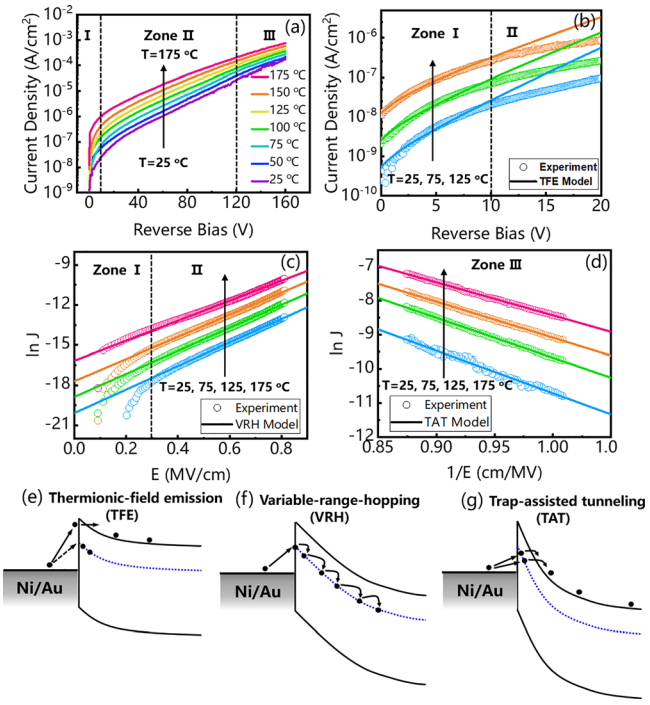

FIG. 2. (a) T-dependent reverse I–V characteristics of the Ref-SBD. (b) Measured reverse I–V characteristics up to 20 V at 25, 75, and 125 °C, and their fitting data based on the TFE model. (c) Measured reverse I–V characteristics and their fitting data based on the (c) VRH model up to 80 V and (d) TAT model from 120 to 160 V. The schematic diagram of reverse leakage near the Schottky interface based on the (e) TFE, (f) VRH, and (g) TAT models.

$$J_{VRH} = J_0 \exp\left[C\frac{eEa}{2kT}\left(\frac{T_0}{T}\right)^{1/4}\right],$$

where J_0 is the zero-field current density, C is a constant, and T_0 is the characteristic temperature. It is worth noting that the extracted Schottky barrier height based on the TFE model at room temperature (~0.71 eV) is lower than that calculated from the forward I–V characteristics at room temperature (~1.12 eV). This implies that some electrons from the anode are, indeed, injected into the defects mini-band instead of the conduction band,[26] as the dotted arrows shown in Fig. 2(e).

As the V_R exceeds 120 V (zone III, the corresponding calculated E is over 1 MV/cm), the reverse leakage of the Ref-SBD exhibits less dependence on the temperature. Considering the strong electric field crowding effect near the junction edge of the Ref-SBD under a large reverse bias, the main leakage may arise from the trap-assisted tunneling (TAT) conduction,[27] which can be expressed by

$$J_{TAT} \propto \exp\left(-\frac{8\pi\sqrt{2qm_n^*}}{3hE}\phi_T\right),$$

where ϕ_T is the trap energy level. The linear relationship between ln$J$ and $1/E$ [Fig. 2(d)] confirms that the dominant leakage comes from the TAT conduction. The strong electric field within the depletion region reduces the lateral distance between the traps and the available states in the conduction band, substantially increasing the probability of electron tunneling,[28] as depicted in Fig. 2(g). The failure devices show the commonly observed destructive holes near the anode edge. The transitions of the dominant leakage mechanisms [Figs. 2(e)–2(g)] are related to the bias-dependent inclination of the energy bands, which affected the carrier transport dynamics. Notably, a self-consistent trap level E_C −0.54 eV is extracted from the data fitting based on the TFE and TAT models. This trap level is very close to the widely reported E_C −0.6 eV for GaN grown on Si.[29–31] The traps might be related to carbon-related defects,[30] or edge-type dislocations.[31]

Figure 3(a) shows the T-dependent reverse I–V characteristics up to the breakdown region for the ArIT-SBD from 25 to 175 °C with a step 50 °C. A large temperature step is beneficial for studying the temperature dependence of the leakage current for various devices. As illustrated in Fig. 3(b), ln$J$ and ln$V$ maintain a linear relationship under a low V_R up to 20 V (ln20 ≈ 3); then, ln$J$ grows super linearly with ln$V$. Moreover, the surface leakage could be ignored in this case, because no correlation is found between the reverse leakage current and the perimeter of the anode (not show here).[32] These curves indicate that the space-charge-limited conduction (SCLC) mechanism dominates the reverse leakage of the ArIT-SBD.[10,22,33,34] The temperature-dependent leakage behavior indicates this is due to a trap-assisted conduction process.[22]

When the V_R is raised above 30 V ($E \sim 0.3$ MV/cm), ln$J$ becomes linearly proportional to E, as shown in Fig. 3(c), implying that VRH conduction-related leakage dominates the reverse leakage of the ArIT-SBD. Meanwhile, the ln$J$ as a function of $T^{-5/4}$ obtained from the experimental data under various large reverse bias (50, 100, 150, and 200 V) exhibits a linear relationship (not shown here), further confirming that the VRH conduction is the main leakage mechanism for the ArIT-SBD under a large V_R.

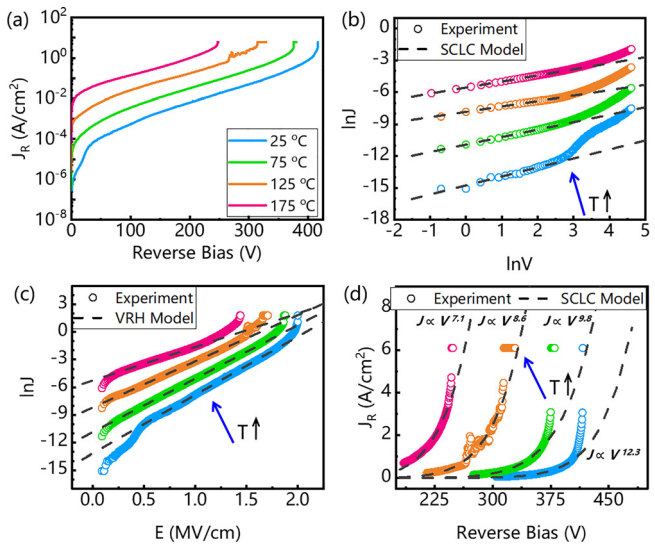

FIG. 3. (a) T-dependent reverse I–V characteristics up to the breakdown region for the ArIT-SBD from 25 to 175 °C with a step 50 °C. Measured reverse I–V curves and their fitting data based on the (b) SCLC model up to 100 V, (c) VRH model. (d) SCLC model at the high reverse bias, following the relation of $J \propto V^n$.

As the V_R exceeds 340 V ($E \sim 1.75$ MV/cm) for the ArIT-SBD, the leakage current grows more rapidly than the expected value based on the VRH model as shown in Fig. 3(c). The well fittings based on the relation of $J \propto V^n$ imply that the dominant leakage and breakdown mechanisms follow the SCLC model,[35] as shown in Fig. 3(d).

Figure 4(a) presents the evolution of the various leakage mechanisms as the reverse bias varies for both the Ref-SBD and ArIT-SBD at room temperature. It can be found clearly that, due to the ArIT, the dominant leakage mechanism for the GaN SBD under a low V_R (~10 V) transforms from TFE to SCLC. It implies that the dominant leakage of the ArIT-SBD originates from the ion-implanted region during the formation of the ArIT, where the injected electrons from the anode edge fill the damage-induced traps in the implanted region,[10,22,34] as the linear relation between ln$J$ and ln$V$ reveals in Fig. 3(b). Meanwhile, the Ohmic-like I–V characteristics under a low V_R also imply that electrons injected from the anode edge into the implanted region hardly experience any Schottky barrier. As a matter of fact, it is very challenging to form a high-quality Schottky contact on a semiconductor surface treated by severe ion bombardment.[10,36] Considering the lateral straggling of the implanted ions toward the GaN below the anode metal, the local Schottky contact between the implanted GaN and anode metal may be degraded and loses the optimized rectifying function.[10,36] In contrast, in the case of the Ref-SBD, the electrons injected from the anode edge also need to cross the Schottky barrier through the TFE process. Therefore, the rapidly growing leakage of the ArIT-SBD under a low V_R goes through the locally degraded Schottky junction between the Schottky metal and implanted GaN, following SCLC model as shown in Fig. 4(b).

With the increment of V_R, the damage-induced traps could be occupied by the injected electrons gradually from the anode metal and become negatively charged.[10] Once the damage-induced traps are filled with electrons,[22,34] a space charge region could be formed around the interface between the negatively charged Ar-implanted region and n^--GaN drift layer,[29] which is similar to the case of p-n junction, as shown in Fig. 5(b). The negatively charged traps could help to deplete the n^--GaN drift layer partially and extend the space depletion region around the ArIT region, which promotes the spreading of the electric potential along the surface.[10] Considering that the electric field strength is proportional to the derivative of the electric potential, that implies the space depletion region around the ArIT region could modify the electric field distribution and alleviate the electric field strength at the junction edge in the GaN SBD.

As the V_R is increased to a high level (~250 V, $E \sim 1.45$ MV/cm), it is noted that the VRH conduction dominates for the ArIT-SBD, and the TAT leakage mechanism does not show up, as shown in Fig. 4(a). This is markedly different from the case of the Ref-SBD without ArIT, in which the peak electric field at the junction edge [Fig. 5(a)] is usually responsible for the tunneling current.[37] The suppression of tunneling current at a high V_R verifies that the ArIT is greatly beneficial to relax the electric field crowding [Fig. 5(b)], which is consist with the previous physics analysis. On the other hand, the dominant leakage mechanism of the ArIT-SBD transforms from SCLC to VRH model, and it indicates that dominant leakage path transforms from the edge degraded Schottky junction through damage-induced traps in the ArIT to central nonimplanted Schottky junction through intrinsic defects/dislocations in bulk GaN.

When the V_R reaches ~340 V for the ArIT-SBD, the leakage current follows the SCLC model, and the dominant leakage mechanism transforms from VRH to SCLC model, as illustrated in Fig. 3(d). Under the high E-field, these high-density charged intrinsic traps in the space depletion region could modulate the spatial E-field profile and affect the carriers transport process. Inversely proportional to the operation temperature,[38] n in the relation of $J \propto V^n$ decreases at the

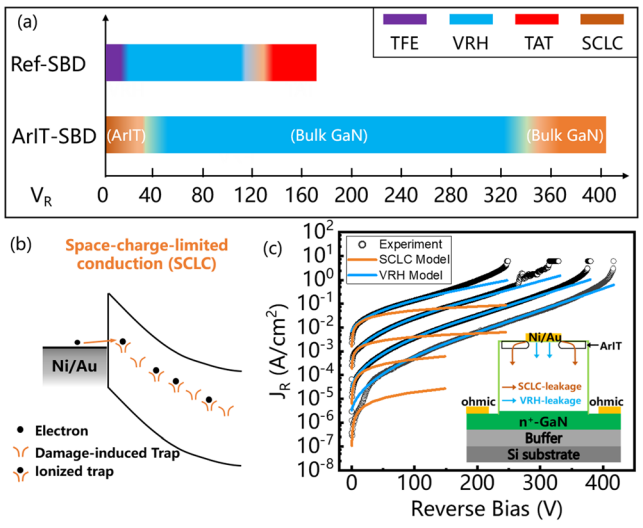

FIG. 4. (a) Schematic diagram of various leakage mechanisms for the Ref-SBD and ArIT-SBD under a reverse bias at 25 °C. (b) The schematic diagram of reverse leakage near the implanted region based on the SCLC model. (c) Measured reverse I–V characteristics and their fitting data based on the VRH and SCLC models for the ArIT-SBD. Inset: the reverse leakage through the edge ArIT region follows the SCLC model, named as the SCLC leakage and through the bulk GaN, named as the VRH-leakage.

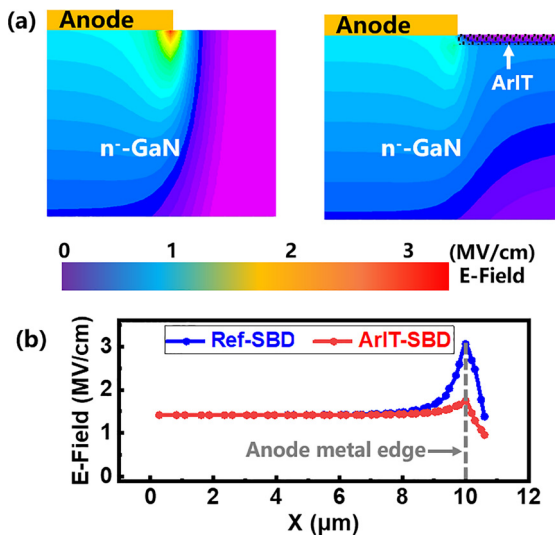

FIG. 5. (a) Simulated electric field distribution in the Ref-SBD and ArIT-SBD at the V_R of 250 V, respectively. (b) Extracted electric field profile near the Schottky junction edge.

elevated temperature. Our analyses on the origins of the reverse VRH- and SCLC-based leakage are consistent with a recent work,[39] which finds that carbon-related defects/traps contribute to the trap-assisted SCLC leakage in the thick GaN grown on Si substrates. The observed destructive morphology in the nonedge region of the failed devices also verifies that the breakdown mechanisms are related to the traps in GaN grown on Si. This trap-assisted SCLC mechanism has been observed in GaN PIN diodes,[35] trench MOS barrier Schottky diodes (TMBSs), and FinFETs under a high V_R.[4,40]

Based on the above analysis, a rapidly growing leakage under a low V_R and the enhanced BV performance could be ascribed to the charging of the damage-induced traps in the ArIT. At the low V_R, neutral traps could be occupied by the injected electrons through the edge degraded Schottky junction from the anode, which leads to a growing rapidly leakage current, following SCLC model. As the V_R increases, these traps are occupied fully and negatively charged. As a result, the charged traps could deplete the drift layer laterally and modulate the electrical potential, leading to a boosted BV for ArIT-SBDs.

The typical leakage current behaviors are summarized in Fig. 6. Basically, with optimized electric field profile at the Schottky junction edge, the leakage and breakdown mechanisms for vertical GaN-on-Si SBDs are limited by material intrinsic defects to a great extent. However, in practice, the electric field crowding effect plays a key role for the vertical GaN SBDs without ET, leading to a high tunneling current assisted by intrinsic traps in GaN or/and Schottky interface traps under a high V_R. Specifically, at the low V_R, the electrode-limited process dominates the electron conduction, such as thermal emission or TFE conduction in the SBDs without ET. Owing to the developed ET, the growing leakage current could be suppressed remarkably.[10] As the V_R increases, the increased electric field assists the leakage following the VRH model through the high-density intrinsic traps, further leading to the occurrence of the tunneling leakage and premature breakdown for the SBDs without ET. By contrast, for vertical SBDs with an advanced ET, due to the effective suppression of the crowding electric field, the VRH conduction could dominate the leakage current up to a high reverse bias, where plenty of electrons are accumulated in the space depletion region. Afterwards, the trap-assisted SCLC process contributes to the leakage current and finally leads to the mature breakdown.

In summary, the physics mechanisms of leakage and breakdown mechanisms for vertical GaN-on-Si SBDs were studied in detail. Through a systematic investigation on the reverse leakage behavior of the devices with and without implanted termination, the widely observed and growing rapidly leakage current at a low reverse bias accompanied by an enhanced BV was clarified. Therefore, this work not only gives an in-depth insight for the leakage mechanisms of vertical GaN-on-Si SBDs but also provides a useful guidance for the design and fabrication of ion implantation-based ET structure for various GaN vertical power devices in future.

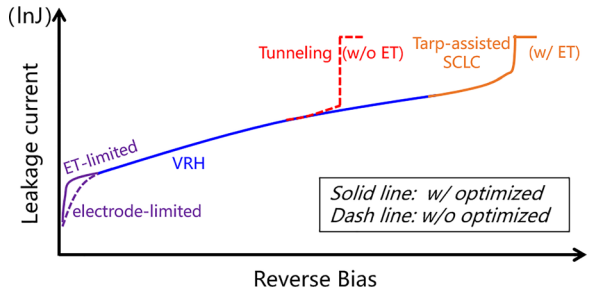

FIG. 6. The evolution schematic of typical leakage/breakdown mechanisms for the vertical GaN-on-Si SBDs with (solid line) and without (dash line) the optimized electric field profile at the Schottky junction edge under the elevated bias.

The authors are grateful for the financial support from Key-Area R&D Program of Guangdong Province (Grant Nos. 2019B010130001, 2019B090917005, 2019B090904002, 2019B090909004, and 2020B010174004), Strategic Priority Research Program of CAS (Grant Nos. XDB43000000 and XDB43020200), Key Research Program of Frontier Sciences, CAS (Grant Nos. QYZDB-SSW-JSC014 and ZDBS-LY-JSC040), CAS Interdisciplinary Innovation Team, National Natural Science Foundation of China (Grant Nos. 61534007, 61775230, 61804162, 61874131, and 62074158), Jiangsu Provincial Key R&D Program (No. BE2020004-2), Natural Science Foundation of Jiangsu Province (Grant No. BK20180253), and Suzhou Science and Technology Program (Grant No. SYG201927). We are thankful for the technical support from Nano Fabrication Facility, Platform for Characterization and Test, and Nano-X of SINANO, CAS.

DATA AVAILABILITY

The data that support the findings of this study are available from the corresponding authors upon reasonable request.

REFERENCES

[1]T. Oka, Jpn. J. Appl. Phys., Part 1 **58**, Sb0805 (2019).
[2]S. Han, S. Yang, R. Li, X. K. Wu, and K. Sheng, IEEE Trans. Power Electron. **34**(6), 5012–5018 (2019).
[3]J. Liu, M. Xiao, R. Zhang, S. Pidaparthi, C. Drowley, L. Baubutr, A. Edwards, H. Cui, C. Coles, and Y. Zhang, IEEE Electron Device Lett. **41**(9), 1328–1331 (2020).
[4]M. Xiao, X. Gao, T. Palacios, and Y. H. Zhang, Appl. Phys. Lett. **114**(16), 163503 (2019).
[5]Y. Zhang, A. Dadgar, and T. Palacios, J. Phys. D **51**(27), 273001 (2018).
[6]R. A. Khadar, C. Liu, L. Zhang, P. Xiang, K. Cheng, and E. Matioli, IEEE Electron Device Lett. **39**(3), 401–404 (2018).
[7]C. Liu, R. Abdul Khadar, and E. Matioli, IEEE Electron Device Lett. **39**(7), 1034–1037 (2018).
[8]S. Han, S. Yang, and K. Sheng, IEEE Electron Device Lett. **39**(4), 572–575 (2018).
[9]S. Yang, S. Han, and K. Sheng, Semicond. Sci. Technol. **36**(2), 024005 (2002).
[10]R. Yin, Y. Li, C. P. Wen, Y. Fu, Y. Hao, M. Wang, and B. Shen, in *2020 32nd International Symposium on Power Semiconductor Devices and ICs (ISPSD)* (IEEE, Piscataway, NJ, 2020), pp. 298–301.
[11]X. Guo, Y. Zhong, J. He, Y. Zhou, S. Su, X. Chen, J. Liu, H. Gao, X. Sun, Q. Zhou, Q. Sun, and H. Yang, IEEE Electron Device Lett. **42**, 473 (2021).
[12]Y. Zhang, J. Zhang, Z. Feng, Z. Hu, J. Chen, K. Dang, Q. Yan, P. Dong, H. Zhou, and Y. Hao, IEEE Trans. Electron Devices **67**(10), 3948–3953 (2020).
[13]H. Zhou, Q. L. Yan, J. C. Zhang, Y. J. Lv, Z. H. Liu, Y. N. Zhang, K. Dang, P. F. Dong, Z. Q. Feng, Q. Feng, J. Ning, C. F. Zhang, P. J. Ma, and Y. Hao, IEEE Electron Device Lett. **40**(11), 1788–1791 (2019).
[14]Y. Y. Gao, A. Li, Q. Feng, Z. Z. Hu, Z. Q. Feng, K. Zhang, X. L. Lu, C. F. Zhang, H. Zhou, W. X. Mu, Z. T. Jia, J. C. Zhang, and Y. Hao, Nanoscale Res. Lett. **14**, 8 (2019).
[15]A. M. Ozbek and B. J. Baliga, IEEE Electron Device Lett. **32**(10), 1361–1363 (2011).
[16]D. Alok, B. J. Baliga, and P. K. McLarty, IEEE Electron Device Lett. **15**(10), 394–395 (1994).

[17]Y. Sun, K. Zhou, Q. Sun, J. Liu, M. Feng, Z. Li, Y. Zhou, L. Zhang, D. Li, S. Zhang, M. Ikeda, S. Liu, and H. Yang, Nat. Photonics **10**(9), 595–599 (2016).
[18]J. Liu, Y. Huang, X. Sun, X. Zhan, Q. Sun, H. Gao, M. Feng, Y. Zhou, M. Ikeda, and H. Yang, J. Phys. D **52**(42), 425102 (2019).
[19]K. Fu, H. Fu, X. Huang, T. Yang, C. Cheng, P. R. Peri, H. Chen, J. Montes, C. Yang, J. Zhou, X. Deng, X. Qi, D. J. Smith, S. M. Goodnick, and Y. Zhao, IEEE J. Electron Devices Soc. **8**, 74–83 (2020).
[20]Y. Zhang, M. Sun, D. Piedra, J. Hennig, A. Dadgar, and T. Palacios, Appl. Phys. Lett. **111**(16), 163506 (2017).
[21]F. Roccaforte, S. Libertino, V. Raineri, A. Ruggiero, V. Massimino, and L. Calcagno, J. Appl. Phys. **99**(1), 013515 (2006).
[22]F. C. Chiu, Adv. Mater. Sci. Eng. **18**, 578168 (2014).
[23]J. Suda, K. Yamaji, Y. Hayashi, T. Kimoto, K. Shimoyama, H. Namita, and S. Nagao, Appl. Phys. Express **3**(10), 101003 (2010).
[24]Y. Zhang, M. Sun, Z. Liu, D. Piedra, J. Hu, X. Gao, and T. Palacios, Appl. Phys. Lett. **110**(19), 193506 (2017).
[25]Y. Zhang, H. Wong, M. Sun, S. Joglekar, L. Yu, N. A. Braga, R. V. Mickevicius, and T. Palacios, in *2015 IEEE International Electron Devices Meeting (IEDM)* (IEEE, Piscataway, NJ, 2015), pp. 35.31.31–35.31.34.
[26]B. Y. Wang, M. Xiao, X. D. Yan, H. Y. Wong, J. H. Ma, K. Sasaki, H. Wang, and Y. H. Zhang, Appl. Phys. Lett. **115**(26), 263503 (2019).
[27]Z. H. Liu, G. I. Ng, S. Arulkumaran, Y. K. T. Maung, and H. Zhou, Appl. Phys. Lett. **98**(16), 163501 (2011).
[28]J. R. Nicholls, S. Dimitrijev, P. Tanner, and J. Han, IEEE Trans. Electron. Devices **66**(4), 1675–1680 (2019).
[29]C. H. Zhou, Q. M. Jiang, S. Huang, and K. J. Chen, IEEE Electron Device Lett. **33**(8), 1132–1134 (2012).
[30]S. DasGupta, M. Sun, A. Armstrong, R. J. Kaplar, M. J. Marinella, J. B. Stanley, S. Atcitty, and T. Palacios, IEEE Trans. Electron Devices **59**(8), 2115–2122 (2012).
[31]A. Armstrong, A. R. Arehart, B. Moran, S. P. DenBaars, U. K. Mishra, J. S. Speck, and S. A. Ringel, Appl. Phys. Lett. **84**(3), 374–376 (2004).
[32]Y. Zhang, M. Sun, H. Wong, Y. Lin, P. Srivastava, C. Hatem, M. Azize, D. Piedra, L. Yu, T. Sumitomo, N. A. de Braga, R. V. Mickevicius, and T. Palacios, IEEE Trans. Electron Devices **62**(7), 2155–2161 (2015).
[33]M. A. Lampert, Phys. Rev. **103**(6), 1648–1656 (1956).
[34]F. C. Chiu, H. W. Chou, and J. Lee, J. Appl. Phys. **97**(10), 103503 (2005).
[35]Y. Zhang, M. Yuan, N. Chowdhury, K. Cheng, and T. Palacios, IEEE Electron Device Lett. **39**(5), 715–718 (2018).
[36]S. Zhu, C. Detavernier, R. L. Van Meirhaeghe, F. Cardon, A. Blondeel, P. Clauws, G. Ru, and B. Li, Semicond. Sci. Technol. **16**(2), 83–90 (2001).
[37]S. Sabuktagin, Y.-T. Moon, S. Dogan, A. A. Baski, and H. Morkoc, IEEE Electron Device Lett. **27**(4), 211–213 (2006).
[38]A. J. Campbell, D. D. C. Bradley, and D. G. Lidzey, J. Appl. Phys. **82**(12), 6326–6342 (1997).
[39]H. Wang, P. C. Hsu, M. Zhao, E. Simoen, A. Sibaja-Hernandez, and J. Wang, IEEE Trans. Electron Devices **67**(11), 4827–4833 (2020).
[40]Y. Zhang, M. Sun, Z. Liu, D. Piedra, M. Pan, X. Gao, Y. Lin, A. Zubair, L. Yu, and T. Palacios, in *2016 IEEE International Electron Devices Meeting (IEDM)* (IEEE, Piscataway, NJ, 2016), pp. 10.12.11–10.12.14.